Appendix B

Maps and billiards

B.1 One-dimensional maps

Even though physically interesting chaotic dynamics requires continuous time flows in state spaces of dimension 3 or higher, we shall nevertheless often find it convenient to illustrate the general principles of chaotic dynamics by examples drawn from discrete time 1-d iterated map dynamics. For dissipative driven flows close to transitions to chaotic dynamics, such as in the period-doubling transition to chaos, chapter 26, this is not a bad approximation, but for us the role of 1-d maps will be mostly didactic. As we are using many different maps throughout the monograph, we collect them all in this section in order to lessen the confusion.

B.1.1 Piecewise-linear 1-d maps

Examples of *piecewise-linear 1-d maps* of the unit interval $x \in [0, 1]$ are

1. A repeller with only one expanding linear branch, and one fixed point $x = 0$, figure B.1 (a):

$$f(x) = \Lambda x\,, \qquad |\Lambda| > 1\,. \tag{B.1}$$

2. The Bernoulli map, figure B.1 (b):

$$f(x) = \begin{cases} f_0(x) = 2x\,, & x \in I_0 = [0, 1/2) \\ f_1(x) = 2x - 1\,, & x \in I_1 = (1/2, 1] \end{cases}\,. \tag{B.2}$$

3. The skew Bernoulli map, figure B.1 (c):

$$f(x) = \begin{cases} f_0(x) = \Lambda_0 x\,, & x \in I_0 = [0, 1/\Lambda_0) \\ f_1(x) = \frac{\Lambda_0}{\Lambda_0 - 1}(x - \frac{1}{\Lambda_0})\,, & x \in I_1 = (1/\Lambda_0, 1] \end{cases} \tag{B.3}$$

symbolic dynamics!coding

4. A 2-branch repeller on two non-overlapping intervals with slopes $\Lambda_0 > 1$ and $\Lambda_1 < -1$, figure B.1 (d):

$$f(x) = \begin{cases} f_0(x) = \Lambda_0 x \,, & x \in I_0 = [0, \Lambda_0] \\ f_1(x) = \Lambda_1(1-x)\,, & x \in I_1 = [\Lambda_1, 1] \end{cases} . \tag{B.4}$$

5. The Ulam tent map, figure B.1 (e):

$$f(x) = \begin{cases} f_0(x) = 2x \,, & x \in I_0 = [0, 1/2) \\ f_1(x) = 2(1-x)\,, & x \in I_1 = (1/2, 1] \end{cases} . \tag{B.5}$$

6. The skew Ulam tent map, figure B.1 (f):

$$f(x) = \begin{cases} f_0(x) = \Lambda_0 x \,, & x \in I_0 = [0, 1/\Lambda_0) \\ f_1(x) = \frac{\Lambda_0}{\Lambda_0 - 1}(1-x)\,, & x \in I_1 = (1/\Lambda_0, 1] \,. \end{cases} \tag{B.6}$$

7. The Cantor map, figure B.1 (g):

$$f(x) = \begin{cases} f_0(x) = 3x \,, & x \in I_0 = [0, 1/3] \\ f_1(x) = 3x - 2\,, & x \in I_1 = [2/3, 1] \end{cases} . \tag{B.7}$$

8. The dike map, figure B.1 (h)

$$f(x) = \begin{cases} f_0(x) = 2x & x \in I_0 = [0, \gamma(K)/2) \\ f_c(x) = \gamma(K) & x \in I_c = [\gamma(K)/2, 1 - \gamma(K)/2] \\ f_1(x) = 2(1-x) & x \in I_1 = [1 - \gamma(K)/2, 1] \end{cases} . \tag{B.8}$$

The dike map is simply the tent map (B.5) with the top sliced off, convenient for coding the symbolic dynamics, as those x values that survive the pruning (see exercise **??**) are the same as for the full tent map (B.5) and available analytically.

need to split figure B.1 into piecewise linear and smooth parts

We shall refer to any unimodal map for which the critical point x_c is mapped onto the unstable fixed point $x_0 = 0$ as an "Ulam" map.

B.1.2 Nonlinear 1-d maps

Some examples of *nonlinear 1-d maps* of the unit interval $x \in [0, 1]$ are

1. A repeller quadratic map, figure B.2 (a):

$$f(x) = 6x(1-x)\,. \tag{B.9}$$

2. The Ulam map, figure B.2 (b):

$$f(x) = 4x(1-x)\,. \tag{B.10}$$

3. The quadratic map on the interval, figure B.2 (c):

$$f(x) = Ax(1-x)\,, \qquad 0 < A < 4\,. \tag{B.11}$$

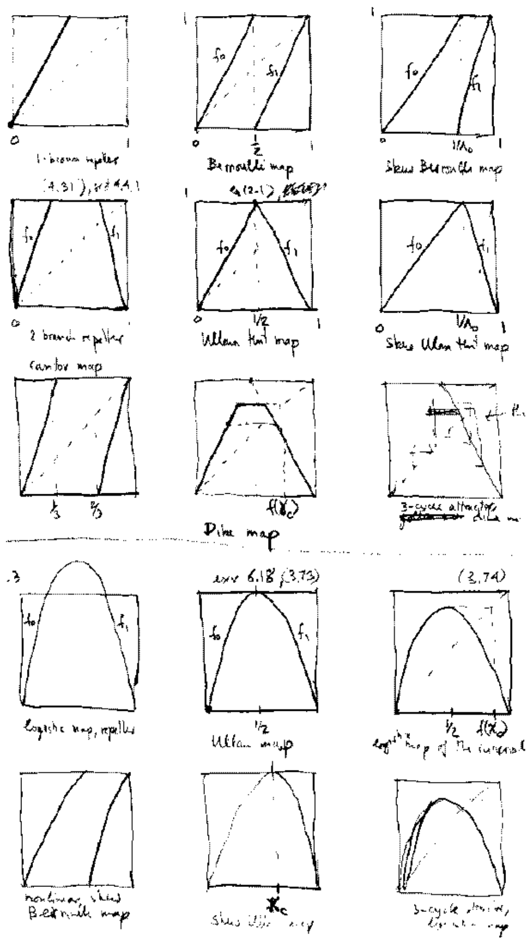

Figure B.1: Examples of *piecewise-linear 1-d maps* of the unit interval $x \in [0, 1]$. (a) repeller with only one expanding linear branch (b) Bernoulli map (c) skew Bernoulli tent map figure B.1 (c) (d) 2-branch repeller on two non-overlapping intervals (e) Ulam tent map (f) skew Ulam tent map (g) Cantor map (h) dike map.

Figure B.2: Examples of nonlinear 1-d maps of the unit interval $x \in [0,1]$. (a) repeller quadratic map(b) Ulam map (c) quadratic map on the interval (e) skew Ulam map (f) nonlinear skew Bernoulli map.

4. The skew Ulam map, figure B.2 (e):

$$x' = \lambda x(1-x)(1-bx) \,, \quad 1/\lambda = x_c(1-x_c)(1-bx_c) \,. \tag{B.12}$$

In our numerical work we fix (arbitrarily) $b = 0.6$.

Hans Henrik + Freddy's map [19.1]; include a figure

5. The nonlinear skew Bernoulli map, figure B.2 (d):

$$\begin{aligned} f_0(x) &= \frac{h-p+\sqrt{(h-p)^2+4hx}}{2h} \,, \qquad x \in [0,p] \\ f_1(x) &= \frac{h+p-1+\sqrt{(h+p-1)^2+4h(x-p)}}{2h} \,, \qquad x \in [p,1] \end{aligned} \tag{B.13}$$

This is a nonlinear perturbation of $(h=0)$ Bernoulli type map (B.3).

The skew Ulam map is a convenient starting point for testing cycle expansions for several reasons:

1. in the $b = 0$ limit it reduces to the quadratic Ulam map (B.10), whose dynamical zeta function is available in explicit analytic form.

2. the symbolic dynamics is a complete binary symbolic dynamics, and all cycles can be easily determined with a combination of inverse iterations and the Newton method.

3. the nth iterate of the map generates a complete binary cover of the unit interval. The strange set has the full Lebesgue measure, so the cycle expansion estimates of the Hausdorff dimension can be tested against the exact value $D_H = 1$.

B.2 Linear fractional maps

An alternative approach to the eigenvalue evaluation is based on observation that the $[2\times2]$ volume preserving , $\det \mathbf{M}_i = 1$, matrix multiplication can be achieved by iteration of linear fractional maps;

this is clumsy; time comes out reversed - change fract lin rep to something more convenient?

$$\begin{aligned} \mathbf{M}_i &= \begin{pmatrix} c_i & a_i \\ d_i & b_i \end{pmatrix} \,, \qquad \rightarrow \quad T_i(z) = \frac{a_i + b_i z}{c_i + d_i z} \,, \\ \mathbf{M}_j\mathbf{M}_i &\rightarrow \quad T_i T_j(z) = \frac{a_i c_j + b_i a_j + (a_i d_j + b_i b_j) z}{c_i c_j + d_i a_j + (c_i d_j + d_i b_j) z} \end{aligned} \tag{B.14}$$

If we represent the translations and the reflections by

billiards!stability
stability!billiards
billiards!with gravity

$$
\begin{aligned}
M_R(x_k) \quad &\rightarrow \quad R_k(z) = r_k + z \,, \\
M_T(x_k) \quad &\rightarrow \quad T_k(z) = \frac{1}{\tau_k + 1/z} \,,
\end{aligned}
\tag{B.15}
$$

the kth segment of the trajectory is represented by

$$
T_k R_k(z) = \frac{1}{\tau_k + \frac{1}{r_k + z}} \,. \tag{B.16}
$$

For the cycle p the iteration yields

$$
z = T_1 R_1 T_2 R_2 \cdots T_{n_p} R_{n_p}(z) = \frac{a_p + b_p z}{c_p + d_p z} \,. \tag{B.17}
$$

For dispersing billiards $r_m > 0$, so all coefficients are positive. The expanding eigenvalue satisfies $|\Lambda_p| + 1/|\Lambda_p| = b_p + c_p$, so cycle eigenvalue is a root of the quadratic equation

obsolete, do as for Madelung

$$
|\Lambda_p| = \frac{b_p + c_p + \sqrt{(b_p + c_p)^2 - 4}}{2} = b_p - d_p z_p \,, \tag{B.18}
$$

alternatively given as the root z_p of the linear fractional representation fixed point condition (B.17). The sign of Λ_p is $(-1)^{n_p}$.

Remark B.1 Sinai-Bunimovich curvature. This is called the Sinai-Bunimovich [6.7, 6.9] continued fraction method of evaluating curvatures. It is equivalent to (6.11), multiplying [2×2] fundamental matrices, the usual method by which the stabilities are evaluated.

B.3 Billiards with gravity: 2 balls on a line

The Hamiltonian for two balls placed vertically on a line is

$$
H = \frac{m_1 v_1^2}{2} + \frac{m_2 v_2^2}{2} + m_1 q_1 + m_2 q_2 \,. \tag{B.19}
$$

We take $q_1 \leq q_2$, place the floor at $q_i = 0$, and fix the mass scale by $m_1 + m_2 = 1$. Following Wojtkowski [6.29], we chose as the 4 coordinates the ball energies and velocities. This choice is convenient, as the (h, v) pair

Make into remark about ergodicity

one can now trace out nt the (h, v) plane the allowed region for fixed energy, and the double-collision line which determines whether next bounce is against the floor, or against the upper ball - just as in the wedge problem in ref. [6.28].

$$
\begin{aligned}
h &= h_1 = \frac{1}{2} m_1 v_1^2 + m_1 q_1 \,, \qquad h_2 = \frac{1}{2} m_2 v_2^2 + m_2 q_2 = -h \\
v &= v_1 - v_2
\end{aligned} \tag{B.20}
$$

is a symplectic pair of coordinates: the energy conservation eliminates $h_2 = -h$, v is transverse to the flow, and $v_1 + v_2$ points along the flow and can be ignored. The equations of motion for the transverse coordinates $x = (h, v)$ are

$$
\frac{d}{dt} h = 0 \,, \qquad \frac{d}{dt} v = 0 \,. \tag{B.21}
$$

The second equation is a consequence of constant acceleration, $\frac{d}{dt} v_i = -1$, so for free fall the flight does not defocus the trajectories.

When the lower ball hits the floor, its velocity reverses direction, $v_1^+ = -v_1^-$. As at the moment of impact $q_1 = 0$, v_1^+ can be expressed in terms of h:

$$
\begin{aligned}
h^+ &= h^- \\
v^+ &= v^- + 2\sqrt{\frac{2h}{m_1}} \,.
\end{aligned} \tag{B.22}
$$

The conservation of energy and momentum yields the velocities and energies after a ball-ball collision:

$$
\begin{aligned}
h^+ &= -h^- + m_1 m_2 (m_1 - m_2) v^2 + 2 m_1 E \\
v^+ &= -v^- \,, \qquad q_1 = q_2 \,.
\end{aligned} \tag{B.23}
$$

The fundamental matrixs can be evaluated by a variation of the symplectic pair of local coordinates (B.20):

$$
\begin{aligned}
\delta h &= m_1 v_1 \delta v_1 + m_1 \delta q_1 \\
\delta v &= \delta v_1 - \delta v_2 \,.
\end{aligned} \tag{B.24}
$$

When the lower ball hits the floor, its velocity reverses direction:

$$
\begin{aligned}
\delta h^+ &= \delta h^- \\
\delta v^+ &= \delta v^- + \sqrt{\frac{2}{m_1 h}} \delta h^- \,.
\end{aligned} \tag{B.25}
$$

In intervals between the ball-ball collisions, the lower ball keeps bouncing with the same fundamental matrix at each bounce, with the stability matrix (4.32) for n bounces given by

$$
M^n(x) = \begin{pmatrix} 1 & 0 \\ n\sqrt{\frac{2}{m_1 h}} & 1 \end{pmatrix} \,. \tag{B.26}
$$

Recheck the α sign here.

The ball-ball collision fundamental matrix follows from (B.23):

billiards!wedge

$$\begin{aligned} \delta h^+ &= -\delta h^- - \alpha \delta v^- , \qquad \alpha = 2 m_1 m_2 (m_1 - m_2) v^- \\ \delta v^+ &= -\delta v^- \\ M(x) &= \begin{pmatrix} -1 & -\alpha \\ 0 & -1 \end{pmatrix} . \end{aligned} \tag{B.27}$$

The two-ball collision must always be followed by one or more bounces of the lower ball against the bottom, hence the natural symbolic dynamics for this problem is n-ary, with the corresponding fundamental matrix given by (B.27) and (B.26)

$$M_n(x) = \begin{pmatrix} 1 & 0 \\ n\sqrt{\frac{2}{m_1 h}} & 1 \end{pmatrix} \begin{pmatrix} -1 & -\alpha \\ 0 & -1 \end{pmatrix} . \tag{B.28}$$

This matrix multiplication can be recast in the continued fraction form, as in (6.14).

B.4 Wedge billiard

The wedge billiard consists of a particle moving in a plane in a constant gravitational field, bouncing elastically between a vertical wall and a plane inclined at angle θ to the vertical axis. θ is the only parameter of the system. The dynamics can be reduced to a two-dimensional map $(X, Y) \to T(X, Y)$, where X and Y are functions of velocity components respectively parallel and perpendicular to the inclined plane at the moment of collision:

$$X = \vec{e}_r \cdot \vec{v} \cos\theta , \quad Y = \vec{e}_\theta \cdot \vec{v} \sin\theta . \tag{B.29}$$

$\vec{e}_r$ is the unit vector pointing along the inclined plane, from the tip of the wedge to the position of the particle; $\vec{e}_\theta$ points perpendicularly out of the plane. The map T is given by:

Maybe should remove $\leq$ from: $(x_t - 2y_t)^2 \cos^2\theta + y_t^2 \sin^2\theta \leq 1$ as one probably needs a different symbol for the pruning front points - just as we have L,C,R for unimodal maps.

$$\begin{aligned} & \qquad \text{if} \quad (X_k - 2Y_k)^2 \cos^2\theta + Y_k^2 \sin^2\theta \leq 1 \\ T_0 \; &: \; \begin{cases} X_{k+1} = X_k - 2Y_k \\ Y_{k+1} = Y_k \end{cases} \\ & \qquad \text{else} \\ T_1 \; &: \; \begin{cases} X_{k+1} = Y_k - X_k - Y_{k+1} \\ Y_{k+1} = \sqrt{2 + 2\xi (Y_k - X_k)^2 - Y_k^2} \end{cases} . \end{aligned} \tag{B.30}$$

Where $\xi = \frac{1-\tan^2\theta}{(1+\tan^2\theta)^2}$. The map T_0 corresponds to two consecutive bounces off the inclined plane, while map T_1 describes the particle bouncing from the inclined plane to the vertical wall and then back again to the inclined plane. The mapping is area preserving in coordinates $(x, y) = (X \cos\theta, Y \sin\theta)$, with the fundamental matrix

$$\begin{aligned} M_0(x_k) &= \begin{pmatrix} 1 & -\frac{c}{s^2}\frac{1}{Y_k} \\ 0 & 1 \end{pmatrix}, \qquad c = \cos\theta\,, \quad s = \sin\theta \\ M_1(x_k) &= \begin{pmatrix} 1 & -\frac{c}{2s^2}\frac{1}{Y_{k+1}} \\ 0 & 1 \end{pmatrix} \begin{pmatrix} -1 & 0 \\ -4\xi\frac{s^2}{c}(Y_k - X_k) & -1 \end{pmatrix} \begin{pmatrix} 1 & -\frac{c}{2s^2}\frac{1}{Y_k} \\ 0 & 1 \end{pmatrix}. \end{aligned} \tag{B.31}$$

The wedge billiard, with Hamiltonian

$$H = \frac{1}{2}(P_1^2 + P_2^2) + Q_2 \tag{B.32}$$

and boundaries given by a vertical wall and a wall inclined at angle θ, is a canonical transformation of the 2-ball system (B.19):

$$\begin{array}{rclrcl} m_1 &=& \sin^2\theta & m_2 &=& \cos^2\theta \\ Q_1 &=& (q_1 - q_2)\sin\theta\,\cos\theta & Q_2 &=& q_1\sin^2\theta + q_2\cos^2\theta \\ P_1 &=& (v_1 - v_2)\sin\theta\,\cos\theta & P_2 &=& v_1\sin^2\theta + v_2\cos^2\theta\,. \end{array} \tag{B.33}$$

There is no point of rotating the tangent coordinates as in (B.33), as the natural expression for the wedge billiard map is in terms of the 2-ball velocities; (B.31) is essentially the same fundamental matrix as (B.28).

B.5 Transfer operators

We rederive here the dynamical zeta function (15.16) by the *transfer operator* technique. This is done only to accomodate the reader versed in statistical mechanics transfer operators; this appendix can be skipped in good conscience by anybody else.

remove ths - repat of the main text?

Consider Mandelbrot's favorite example of a fractal, the Cantor set. The set is generated by a single rule: replace a "mother" interval l by two "daughters" of length $l/3$; repeat this replacement *ad infinitum.* Given the rule, one can immediately compute the Hausdorff dimension; at nth level the set can be covered with 2^n intervals of size 3^{-n}, hence $D = \log 2/\log 3$.

where are the dimensions defined?

A transfer operator is a generalization of such rule to non–wandering sets for which the dynamics generates an infinity of scales, not just a single scale as in the Cantor set case. For example, for a repeller like the one illustrated in figure 11.8 the dynamics associates with each "mother" interval l_m, $m = s_2 s_3 \cdots s_n$, two "daughter" intervals l_d, $d = 0s_2 \cdots s_n$,

$1s_2 \cdots s_n$, at the next level of resolution. The transfer operator appropriate to the evaluation of (19.2) is defined by the set of daughter/mother ratios

$$T_{dm} = l_d / l_m \tag{B.34}$$

For the Cantor set $T_{dm} = 1/3$ for all d; for a generic dynamical non–wandering set T_{dm} takes on infinity of values. The sum (19.2) can now be expressed in terms of products of transfer operators:

$$\Gamma_n = \sum_{s_1 s_2 \cdots s_n} T_{s_1 s_2 \cdots s_n, s_2 \cdots s_n} T_{s_2 \cdots s_n, s_3 \cdots s_n} \cdots T_{s_n,}. \tag{B.35}$$

As it stands, this is a purely formal rewrite of (19.2); the "mother" to "daughters" relations place the pieces of a non–wandering set onto a hierarchical tree, and that can be done in various ways. To proceed, we require that the tree provide a hierarchical nesting of the scaling ratios in the following sense: the value of $T_{s_1 s_2 \cdots s_n, s_2 \cdots s_n}$ should depend strongly on the head of the symbol sequence $s_1 s_2 \cdots$, and weakly on the tail $\cdots s_{n-1} s_n$. More precisely, we assume that the specification of first k symbols determines $T_{s_1 s_2 \cdots s_n, s_2 \cdots s_n}$, $n > k$, within accuracy Δ_k

$$T_{s_1 s_2 \cdots s_n, s_2 \cdots s_n} = \tilde{T}^{(k)}_{s_1 s_2 \cdots s_k, s_2 \cdots s_{k+1}} + O(\Delta_k), \tag{B.36}$$

and that $|\Delta_k|$ decrease monotonically towards zero with increasing k. Here $\tilde{T}^{(k)}$ is an approximate "mean" scaling for all T_{dm} with the same first k symbols. Replacing the infinite number of scaling ratios (B.34) by a finite matrix $\tilde{T}^{(k)}$ amounts to approximating the non–wandering set by a Cantor set with a finite number of scales.

An example of such hierarchy is the 1-d repeller of figure 11.8, for which $T_{dm} \approx 1/|f'(x)|$, where $f'(x)$ is a slope of the mapping evaluated at a point x inside the dth neighborhood. With the labeling conventions of figure 11.8, the points whose itineraries have the same head $s_1 s_2 \ldots s_n$ are spatially close, and hence the associated derivatives and transfer matrix elements are close.

Now we can study the transfer operator T as a limit of $\tilde{T}^{(k)}$ finite matrix approximations. For example, for the binary labeled repeller of figure 11.8, $k = 2$ level approximation to T is given by

explain the dynamics is a bit-shift.

$$\tilde{T}^{(2)} = \begin{bmatrix} \tilde{T}_{00.00} & \tilde{T}_{00.01} & 0 & 0 \\ 0 & 0 & \tilde{T}_{01.10} & \tilde{T}_{01.11} \\ \tilde{T}_{10.00} & \tilde{T}_{10.01} & 0 & 0 \\ 0 & 0 & \tilde{T}_{11.10} & \tilde{T}_{11.11} \end{bmatrix}$$

list also 8 x 8 matrix?

For binary symbolic dynamics $\tilde{T}$ is in general a sparse matrix, as the only nonvanishing entries in the $m = s_2 s_3 \ldots s_{k+1}$ column of $\tilde{T}_{dm}$ are in the rows $0s_2 \ldots s_k$ and $1s_2 \ldots s_k$.

In the kth order approximation the sums in (B.35) reduce to matrix multiplication

$$\begin{aligned}\Gamma_n &\approx \Gamma_n^{(k)} = \sum_{s_1 s_2 \cdots s_n} \tilde{T}^{(k)}_{s_1 s_2 \cdots s_k, s_2 \cdots s_{k+1}} \tilde{T}^{(k)}_{s_2 \cdots s_{k+1}, s_3 \cdots s_{k+2}} \cdots T_{s_n,.} \\ &= \sum_{s_1 s_2 \cdots s_k} \sum_{\delta_1 \cdots \delta_k} \left(\tilde{\mathbf{T}}^{n-k}_{(k)}\right)_{s_1 s_2 \cdots s_k, \delta_1 \cdots \delta_k} l_{\delta_1 \cdots \delta_k}, \ . \end{aligned} \qquad \text{(B.37)}$$

Here $\vec{l}$ is the vector of all intervals l_i at the kth level. It plays the same role as the prefactors a_i in (1.4); in the $n \gg k$ limit, the kth level approximation (B.37) is dominated by the leading eigenvalue of $\tilde{T}^{(k)}$

$$\Gamma_n^{(k)} \propto [\lambda^{(k)}_{max}]^n$$

and, as far as the $n \to \infty$ limit is concerned, the preasymptotic intervals $\vec{l}^{(k)}$ contribute only an irrelevant prefactor (unless $\vec{l}^{(k)}$ happens to be normal to the leading eigendirection of $\tilde{T}^{(k)}$). This method of evaluating sums is familiar from statistical mechanics, whence the designation "transfer operator".

B.5.1 Perron-Frobenius-Ruelle theory

The transfer operators were introduced by Ruelle [16.12] as a generalization of the transfer matrices of equilibrium statistical mechanics. For $\beta = 0$ the evolution operator (10.23) is the kernel of the Perron-Frobenius operator (9.27). For the generalized evolution operators it presumably suffices to refer to Ruelle, who introduced [16.9] the *Ruelle-Araki operator*

recheck the ref. [16.9], use Ruelle's original notation?

$$\left(\mathcal{L}^t \circ \rho\right)(x) = \sum_{y=f^{-t}(x)} e^{A(y)} \rho(y) \,. \qquad \text{(B.38)}$$

and who always defines his dynamical zeta functions weighted by multiplicative factors; later papers only rediscover that.

In the mathematical literature, the dominant eigenvalue of the $\mathcal{L}$ operator is related to the averages of the dynamical system by using a theorem of Ruelle (or one of its extensions). Inspired by the statistical mechanics of spin systems, Ruelle extended the Perron-Frobenius theorem for matrices to operators in Banach spaces of bounded functions. He uses the evolution operator introduced in (10.24) with $\beta = 0$ and shows that it can be used to compute the averages of the function h the operator acts on. To do that he assumes that the operator has an isolated largest eigenvalue. With that assumption, he shows that the operator has an adjoint operator acting on the space of measures and that the measure associated with the largest eigenvalue is the invariant measure of the system. A theorem (the Perron-Frobenius-Ruelle theorem) shows that averages of h with this measure can be computed by projecting the function onto the eigenspace of this largest eigenvalue.

The method we use is slightly different. We do not use the action of the operator to compute the averages, but rather rely on the eigenvalue having a few derivatives around $\beta = 0$. The function we want to average is incorporated directly into the definition of the evolution operator; different averages require different operators. The approach is more in the spirit of statistical mechanics, in that we compute a function $s(\beta)$ that is assumed to have a few derivatives with respect to β. That this function exists can be derived from an application of the extensions of Ruelle-Bowen results.

RM: add references to this all